Grid Convergence Error Analysis for Mixed-Order Numerical Schemes

Christopher J. Roy[†]
Sandia National Laboratories[*]
P. O. Box 5800, MS 0825
Albuquerque, NM 87185-0825

Abstract

New developments are presented in the area of grid convergence error analysis for mixed-order numerical schemes. A mixed-order scheme is defined here as a numerical method where the formal order of the truncation error varies either spatially (e.g., at a shock wave) or for different terms in the governing equations (e.g., third-order convection with second-order diffusion). The case examined herein is the Mach 8 inviscid flow of a calorically perfect gas over a spherically blunted cone. This flowfield contains a strong bow shock wave where the formally second-order numerical scheme is reduced to first order via a flux limiting procedure. The proposed mixed-order error analysis method allows for non-monotonic behavior in the solution variables as the mesh is refined. Non-monotonicity in the local solution variables is shown to arise from a cancellation of first- and second-order error terms for the present case. An error estimator is proposed based on the mixed-order analysis and is shown to provide good estimates of the actual error when the solution converges non-monotonically with grid refinement.

---

† Senior Member of Technical Staff, E-mail: cjroy@sandia.gov, Senior Member AIAA
* Sandia is a multiprogram laboratory operated by Sandia Corporation, a Lockheed Martin Company, for the United States Department of Energy under Contract DE-AC04-94AL85000.

Nomenclature

DE	discretization error
F_s	factor of safety for error estimators *(F_s = 3)*
f	general solution variable
g_i	i^{th} order error term coefficient
h	normalized measure of grid spacing *($h_k = [N_1/N_k]^{1/2}$)*
N	number of mesh cells
M	Mach number
p	spatial order of accuracy; pressure, N/m^2
R	gas constant, *J/kg·K* (R = 296.8 *J/kg·K*)
R_N	nose radius (R_N = 0.00508 *m*)
r	grid refinement factor
x	axial coordinate, *m*
y	radial coordinate, *m*
$\varepsilon_{k+1,k}$	difference between solution variable on mesh k+1 and mesh k
γ	ratio of specific heats *(γ = 1.4)*

Subscripts and Superscripts

exact	exact continuum value
k	mesh level (k = 1, 2, 3, etc., fine to coarse)
n	flowfield node index
~	estimated value to order h^{p+1}

Introduction

As computers become faster and algorithms more efficient, computational fluid dynamics (CFD) has enormous potential to contribute to the design, analysis, and certification of engineering systems. However, simulation results are often regarded with skepticism by the engineering community as a whole. Judging by the results of numerous validation studies,[1-4] this lack of confidence in CFD is not surprising. To quote Hutton and Casey [2], "the results of such exercises can be highly user-dependent even when the same CFD software with the same models is being used." Oftentimes, when a number of users do obtain the same results, these results do not agree with the experimental data. In order for CFD to achieve its potential, more work must be done to quantify the accuracy of simulation results.

Verification and validation[5,6] provides a framework for rigorously assessing the accuracy of CFD simulations. Verification deals purely with the mathematics of a chosen set of equations, and can be thought of as "solving the equations right." Validation, on the other hand, entails a comparison to experimental data (i.e., real world observations) and is concerned with "solving the right equations." With regards to the sequence, verification must be performed first for quantitative validation comparisons to be meaningful. Error types that are quantified in verification activities include coding errors (i.e., mistakes), incomplete iterative convergence error, round-off error, far-field boundary error, temporal convergence error, and grid convergence (or discretization) error. This last source of error is related to the adequacy of the computational mesh employed and is the focus of the current effort.

Some terms related to the order of accuracy are now defined. The formal order of accuracy of a given numerical scheme is defined as the lowest order term in the truncation error (i.e., the difference between the continuum partial differential equation and the discretized equations). The

truncation error can be determined by *a priori* substitution of Taylor-series expansions into the discretized equations.[7] A mixed-order scheme is defined here as a scheme in which two terms of different order in the truncation error are of similar magnitude over the range of mesh densities examined. In the current work, a limiter is employed to reduce the formally second-order accurate numerical scheme to first order in the vicinity of shock waves. Finally, the observed order of accuracy is the order as determined by an *a posteriori* examination of the solution(s). The observed order of accuracy will not necessarily be equal to the formal order, especially when the solutions are outside of the asymptotic grid convergence range.

For complex problems, the most reliable methods for assessing the grid convergence errors in the solution to partial differential equations are *a posteriori* methods based on Richardson Extrapolation.[5] Roache[8] has proposed the Grid Convergence Index (*GCI*) as a uniform method for reporting the results of grid refinement studies. As a minimum requirement for estimating solution accuracy, two grid solutions are used along with a knowledge of the formal order of accuracy of the numerical scheme to produce an error estimate in the solution properties. However, this minimum requirement can be misleading when the observed order of accuracy differs from the formal order of accuracy.

Error analysis methods for high-speed compressible flows can be complicated by the presence of shock waves. The most common numerical methods used for high-speed flows are characteristic-based upwind methods. For steady flows, methods that are second order in space are often employed due to their favorable mixture of accuracy and numerical stability. In order to prevent nonphysical oscillations, most upwind schemes employ limiters which reduce the spatial accuracy to first order through shock waves. In fact, Godunov showed that the capturing of a discontinuity without oscillation required that the spatial accuracy of the scheme reduce to first order.[9] The

presence of both second- and first-order spatial accuracy in a solution can greatly complicate grid convergence analyses.

Carpenter and Casper[10] conducted a careful study of the grid convergence behavior for a two-dimensional hypersonic blunt-body flow. Their study employed higher-order methods and omitted any flux limiting at the shock wave. While the numerical schemes they employed were formally third and fourth order, they found that the spatial order of accuracy always reverted to first order on sufficiently refined meshes. Their findings indicate that even without the use of flux limiters to reduce the spatial order of accuracy at discontinuities, the information is passed through the shock wave in a first-order manner (at least in two dimensions and higher). Similar results have been observed by other authors.[11-13] For shock-containing flows, it is surmised that the local truncation error reduces to first order at the discontinuity, regardless of the use of flux limiters. Since the truncation error determines the order of the method, this spatial variation results in a first-order asymptotic behavior as the cell size approaches zero. When the solutions exhibit a clear asymptotic behavior at the formal order of the scheme, followed by a first-order asymptotic range, then the numerical method is herein classified as a mixed-order scheme. It should be noted that if the local discretization error contains any first-order terms, however small, then the mathematical classification of the scheme is technically first order since this first-order term will dominate as the grid spacing approaches zero.

In addition to flows with shock waves, there are many other examples of mixed-order numerical schemes. Leonard's QUICK scheme[14] employs a third-order accurate convective operator and standard second-order central differences for diffusion. Celik and Zhang[15] and Celik and Karatikin[16] examined a subsonic backward-facing step problem with a numerical scheme which used central differences for the diffusion terms, but was a mixture of first-order upwind and sec-

ond-order central difference for the convective terms. A mixed-order behavior can also occur for cases where the transport properties undergo large, abrupt changes, such as at the interface between two porous media.[5]

Previous work by Roy et al.[17,18] and Roy[19] verified the presence of both first- and second-order errors for a laminar hypersonic blunt-body flow when a formally second-order numerical scheme was used in conjunction with flux limiting at the shock wave. It was shown that the use of a mixed-order numerical scheme resulted in non-monotonic convergence of certain flow properties as the mesh was refined. This non-monotonic grid convergence behavior was found to occur when the first- and second-order error terms were of opposite sign, thus leading to error cancellation. Non-monotonic grid convergence has been observed by a number of other authors. For example, Celik and Karatekin[16] examined the flow over a backward facing step using the k-ε turbulence model with wall functions. These authors found significant non-monotonicity in both the velocity and turbulent kinetic energy profiles as the grid was refined.

The main goal of this work is to explore, in detail, the behavior of a mixed first- and second-order numerical scheme as the grid is refined. A secondary goal is to develop an error estimator which can be applied to such schemes. The test problem used is the Mach 8 inviscid flow of a calorically perfect gas ($\gamma = 1.4$) over a spherically-blunted cone. This flowfield contains a strong bow shock wave where the formally second-order spatial discretization reduces to first order.

Computational Model

The computational fluid dynamics code used herein is SACCARA, the Sandia Advanced Code for Compressible Aerothermodynamics Research and Analysis. The SACCARA code was developed from a parallel distributed memory version[20-23] of the INCA code, originally written by Amtec Engineering. For the present simulations, the SACCARA code is used to solve the Eul-

er equations for conservation of mass, momentum, and energy for axisymmetric flow. The calorically perfect gas assumption is made with $\gamma = 1.4$, and the gas is further assumed to be composed of diatomic nitrogen ($R = 296.8$ *J/kg·K*). The governing equations are discretized using a cell-centered finite-volume approach. The convective fluxes at the interface are calculated using the Steger and Warming[24] flux vector splitting scheme. Second-order reconstructions of the interface fluxes are obtained via MUSCL extrapolation.[25] A flux limiter is employed which reduces the spatial discretization to first order in regions of large second derivatives of pressure and temperature. This limiting process is used to prevent oscillations in the flow properties at shock waves. The use of flux limiting results in a mixture of first- and second-order accuracy in space. The implications of the mixed-order scheme on the convergence behavior of the method as the grid is refined will be discussed in detail.

The SACCARA code employs a massively parallel distributed memory architecture based on multi-block structured grids. The solver is a Lower-Upper Symmetric Gauss-Seidel scheme based on the works of Yoon et al.[26,27] and Peery and Imlay,[28] which provides for excellent scalability up to thousands of processors.[29] A number of code verification studies provide confidence that the SACCARA code is free from coding errors. These studies include comparison to established numerical benchmark solutions[17,18] as well as code to code comparisons with Navier-Stokes[17,18,30] and Direct Simulation Monte Carlo[31,32] approaches. The simulations presented herein were run using a single 400 MHz processor of a Sun Enterprise 10000 shared-memory machine.

Extrapolation Techniques

When a differential equation is solved numerically, the discretization error on mesh level k may be written as

$$DE_k = f_k - f_{exact} \tag{1}$$

where f_k is a discrete solution value on mesh level k and f_{exact} is the exact solution to the continuum partial differential equation. Equation (1) may be applied on a point-by-point basis locally within the domain or to global quantities such as lift and drag. The following development is based on a series expansion[5] of the discretization error which, for a uniform mesh, may be rewritten as

$$f_k = f_{exact} + g_1 h_k + g_2 h_k^2 + g_3 h_k^3 + O(h_k^4) \tag{2}$$

where g_i is the ith-order error term coefficient and h_k is some measure of the grid spacing on mesh k. For a formally second-order scheme, the g_1 coefficient will be zero. The general procedure is to write Eq. (2) for a number of different mesh levels and solve for an approximation to f_{exact} and the dominant error term coefficient. In certain cases, an "observed" order p is also determined as part of the error analysis. It should be noted that Eq. (2) is strictly valid only on uniform Cartesian meshes, with the application to curvilinear meshes (or their finite-volume equivalent) dependent on the quality of the coordinate transformation. Without loss of generality, the fine grid spacing is normalized to unity (i.e., $h_1 = 1$), and the grid refinement factor is defined as

$$r_{k,\,k+1} = h_{k+1} / h_k \tag{3}$$

Two of the required assumptions for using these extrapolation methods are that the solutions must be in the asymptotic grid convergence range (i.e., the higher order terms in Eq. (2) are small) and that the solutions must be smooth. The extrapolated solution can be used in one of two ways: to estimate the error of the discrete solutions, or simply as a more accurate solution. This author recommends the former since the latter tends to magnify spatial discretization error, round-off error, and incomplete iterative convergence error. Furthermore, even if the original numerical scheme

locally conserves some properties such as mass, momentum, or energy, the extrapolated solution will not necessarily be conservative.

Standard Richardson Extrapolation

In the early 1900's, Richardson[33,34] developed a method of extrapolating two discrete second-order solutions to yield a fourth-order accurate solution. The solutions were obtained on a fine grid with spacing h_1 and a coarse grid with spacing h_2, with $h_2/h_1 = 2$ (i.e., grid doubling/halving). The fourth-order accuracy of the extrapolated solution arose from the exclusive use of central differences, which contain only even powers in the expansion given in Eq. (2). Unless central differences are used exclusively, the odd terms should be included. Thus, for a second-order numerical scheme, the two discrete solutions may be generally written as

$$\begin{aligned} f_1 &= f_{exact} + g_2 h_1^2 + O(h_1^3) \\ f_2 &= f_{exact} + g_2 h_2^2 + O(h_2^3) \end{aligned} \tag{4}$$

By neglecting the terms of order h^3 and higher, the above system can be solved for approximations to f_{exact} and g_2 (the coefficient of the second-order error term)

$$\tilde{g}_2 = \frac{f_2 - f_1}{3h_1^2} \tag{5}$$

$$\tilde{f}_{exact} = f_1 + \frac{f_1 - f_2}{3} \tag{6}$$

where the overtilde (~) denotes approximate values which neglect higher-order terms. Defining the difference in two successive grid levels as

$$\varepsilon_{21} = f_2 - f_1 \tag{7}$$

and taking $h_1 = 1$, Eqs. (5) and (6) reduce to

$$\tilde{g}_2 = \varepsilon_{21}/3$$
$$\tilde{f}_{exact} = f_1 - \varepsilon_{21}/3 \tag{8}$$

Generalized Richardson Extrapolation

The above Richardson Extrapolation technique can be generalized to arbitrary grid refinement factor r and order p following Roache.[5] The series representation is written as

$$f_1 = f_{exact} + g_p h_1^p + O(h_1^{p+1})$$
$$f_2 = f_{exact} + g_p h_2^p + O(h_2^{p+1}) \; . \tag{9}$$

Approximating the above equations by dropping the higher-order terms and then solving for the p^{th}-order error coefficient g_p and the exact solution f_{exact} results in

$$\tilde{g}_p = \frac{\varepsilon_{21}}{r^p - 1} \tag{10}$$

$$\tilde{f}_{exact} = f_1 - \frac{\varepsilon_{21}}{r^p - 1} \tag{11}$$

where $r = r_{12}$ from Eq. (3). In this case, the order of the discretization p must be assumed *a priori* since only two solutions are used. The above estimates will, in general, be $(p+1)^{\text{th}}$-order accurate.

In addition to using the extrapolated values to estimate the errors in the discrete solutions, it is strongly recommended that the order of accuracy also be verified. The standard method for order verification requires that all three grid solutions be in the asymptotic grid convergence range. The series representation is now expressed as

$$f_1 = f_{exact} + g_p h_1^p + O(h_1^{p+1}) \tag{12}$$

$$f_2 = f_{exact} + g_p h_2^p + O(h_2^{p+1}) \tag{13}$$

$$f_3 = f_{exact} + g_p h_3^p + O(h_3^{p+1}) \tag{14}$$

If the higher order terms are neglected, then the above equations can be solved for approximations to the order p, g_p, and f_{exact} to give

$$\frac{r_{12}^{\tilde{p}} - 1}{r_{12}^{\tilde{p}} r_{23}^{\tilde{p}} - 1} = \frac{\varepsilon_{21}}{\varepsilon_{21} + \varepsilon_{32}} \tag{15}$$

$$\tilde{g}_p = \frac{\varepsilon_{21}}{r_{12}^{\tilde{p}} - 1} \tag{16}$$

$$\tilde{f}_{exact} = f_1 - \frac{\varepsilon_{21}}{r_{12}^{\tilde{p}} - 1} \ . \tag{17}$$

Notice that Eq. (15) is transcendental in $\tilde{p}$ and thus must be solved iteratively (see Ref. 5), and that Eqs. (16) and (17) correspond to Eqs. (10) and (11). For the case when $r_{12} = r_{23} = r$ (i.e., constant grid refinement factor), Eq. (15) reduces to

$$\tilde{p} = \frac{\ln(\varepsilon_{32}/\varepsilon_{21})}{\ln(r)} \tag{18}$$

This last equation was used by de Vahl Davis[35] to solve for the "observed" order of accuracy for the natural convection in a square cavity.

When the three discrete solutions do not converge monotonically as the grid is refined, then $\varepsilon_{32}/\varepsilon_{21} < 0$ and Eq. (18) is therefore undefined. Celik and Karatekin[16] addressed the issue of non-monotonic, or "oscillatory," grid convergence by inserting a negative sign in front of the g_p coefficient in Eq. (13) (the medium mesh). However, there is no mathematical justification for such a procedure. This article will present both an analysis method and an error estimation technique for dealing with non-monotonic grid convergence.

Mixed 1st + 2nd Order Extrapolation

For the case when both first- and second-order error terms are included,[17-19] three discrete so-

lutions are needed, where the series representation is written as

$$\begin{aligned} f_1 &= f_{exact} + g_1 h_1 + g_2 h_1^2 + O(h_1^3) \\ f_2 &= f_{exact} + g_1 h_2 + g_2 h_2^2 + O(h_2^3) \\ f_3 &= f_{exact} + g_1 h_3 + g_2 h_3^2 + O(h_3^3) \end{aligned} \tag{19}$$

The inclusion of more than one error term in the expansion is not a new concept. For example, see Ref. 36 for a discussion of Romberg interpolation as applied to the trapezoidal rule. For arbitrary mesh refinement, the above equations may be solved for approximations to g_1, g_2, and f_{exact} to yield

$$\begin{aligned} \tilde{g}_1 &= \frac{\varepsilon_{32}(1 - r_{12}^2) + \varepsilon_{21} r_{12}^2 (r_{23}^2 - 1)}{r_{12}(r_{12} - 1)(r_{23} - 1)(r_{12} r_{23} - 1)} \\ \tilde{g}_2 &= \frac{\varepsilon_{32}(r_{12} - 1) - \varepsilon_{21} r_{12}(r_{23} - 1)}{r_{12}(r_{12} - 1)(r_{23} - 1)(r_{12} r_{23} - 1)} \\ \tilde{f}_{exact} &= f_1 + \frac{\varepsilon_{32}(r_{12} - 1) - \varepsilon_{21}(r_{12} r_{23}^2 - r_{12} - r_{23} - 1)}{(r_{12} - 1)(r_{23} - 1)(r_{12} r_{23} - 1)} \end{aligned} \tag{20}$$

For the case of a constant grid refinement factor, the above equations simplify to

$$\tilde{g}_1 = \frac{r^2 \varepsilon_{21} - \varepsilon_{32}}{r(r-1)^2} \tag{21}$$

$$\tilde{g}_2 = \frac{\varepsilon_{32} - r\varepsilon_{21}}{r(r+1)(r-1)^2} \tag{22}$$

$$\tilde{f}_{exact} = f_1 + \frac{\varepsilon_{32} - (r^2 + r - 1)\varepsilon_{21}}{(r+1)(r-1)^2} \tag{23}$$

and for $r = 2$, these equations further reduce to

$$\begin{aligned} \tilde{g}_1 &= (-\varepsilon_{32} + 4\varepsilon_{21})/2 \\ \tilde{g}_2 &= (\varepsilon_{32} - 2\varepsilon_{21})/6 \\ \tilde{f}_{exact} &= f_1 + (\varepsilon_{32} - 5\varepsilon_{21})/3 \end{aligned} \tag{24}$$

The above estimates are generally third-order accurate. A third-order error term could be easily included by simply adding another mesh level (see Ref. 19 for details).

Smooth Flow Test Case

In order to verify that the SACCARA code does indeed produce second-order accuracy in space, a test problem with smooth flow is first examined. The inviscid flow of a calorically perfect gas through an axisymmetric nozzle was simulated using five mesh levels: 400×160, 200×80, 100×40, 50×20, and 25×10 cells. The coarse grids were generated from the fine grid by eliminating every other grid line successively in each direction ($r = 2$). The 100×40 cell mesh is shown in Fig. 1 along with Mach number contours. The grids lines are orthogonal to the domain boundaries and equally spaced in the axial direction. The radial height of the cells is a function of the axial coordinate only. The outer wall of the nozzle is given by the following relationship

$$y = 0.005 + 0.195x^2 - 0.13x^3 \tag{25}$$

and the Mach number varies from near unity at the throat ($x = 0$) to approximately five at the outflow. Symmetry is enforced along the x-axis, while tangent flow with zero normal pressure gradient is enforced at the nozzle outer wall.

The observed order of accuracy of the method is estimated by examining the behavior of various norms of the spatial error. In order to calculate error norms, local estimates of the exact solution are required. Estimates of the exact solution were obtained by extrapolating the solutions using the two finest meshes (restricted onto the coarsest 26×11 node mesh) and the second-order

extrapolation method presented in Eq. (8). The L_1 and L_2 norms were then calculated as follows:

$$\mathrm{L}_1 \text{ norm}_k = \frac{\sum_{n=1}^{N} \left| f_{k,n} - \tilde{f}_{exact,n} \right|}{N}$$
$$\mathrm{L}_2 \text{ norm}_k = \left(\frac{\sum_{n=1}^{N} \left| f_{k,n} - \tilde{f}_{exact,n} \right|^2}{N} \right)^{1/2} \tag{26}$$

where k indicates the mesh level and n is summed over the N points used in the norm calculation. In this case, all of the nodal mesh points were used including boundary points. Although not employed in the current work, Roache and Knupp[37] developed a method for obtaining estimates of the exact solution on the fine mesh points.

The norms of the discretization error are given in Fig. 2 for the five grid levels plotted on a log-log scale. The cell spacing parameter h is normalized to unity on the fine mesh, thus the discrete solutions fall at h = 1, 2, 4, 8, and 16. Also shown in the figure are the first- and second-order slopes. The norms are shown to drop in a second-order manner as the grid is refined (i.e., from right to left). This test case confirms that the numerical scheme is, indeed, second-order accurate in space for inviscid smooth problems.

Hypersonic Blunt Body Case

Flowfield Conditions and Grids

The problem of interest is the Mach 8 inviscid flow of a calorically perfect gas (γ = 1.4 and R = 296.8 *J/kg·K*) over a sphere-cone geometry. The nose radius R_N is 0.00508 *m* and the half-angle of the cone is 10 *deg*. The conditions used in these simulations are presented in Table 1. Solutions were obtained for eight grid refinement levels, from Mesh 1 (1024×512 cells) to Mesh 8

(8×6 cells), with each successive grid level found by eliminating every other grid line in the two spatial dimensions (i.e., grid halving). The only exception is Mesh 8, where two additional points were added to the outer boundary in order to capture the shock wave on this coarse mesh. The meshes used in this study do not employ clustering and are summarized in Table 2. For the finest mesh, the spacing normal to the wall varies from 3.5×10^{-6} *m* at the stagnation point ($x/R_N = 0$) to 1.6×10^{-5} *m* at the end of the body ($x/R_N = 2$). The spacing along the surface is approximately constant at 1.4×10^{-5} *m* for the fine mesh. The meshes were generated such that the grid lines are orthogonal to all domain boundaries. The velocity, pressure, and temperature were held constant at the inflow boundary, a zero gradient condition was used at the outflow, and symmetry was enforced at the y = 0 boundary. A tangent flow condition was enforced along the body along with a zero gradient condition for pressure which strictly holds for straight walls. All boundary conditions are implemented is a second-order manner.

A contour plot of Mach number is presented in Fig. 3 along with the flowfield mesh. The 64×32 mesh (Mesh 5) is shown for clarity. A strong shock wave occurs in the domain roughly halfway between the body and the outer boundary. Along the stagnation streamline ($y/R_N = 0$), the shock is normal to the *y*-axis and is effectively grid aligned. For the remainder of the domain, the shock is not aligned with the mesh. In addition, no effort was made to cluster the grid to the shock. For plotting purposes, the spatial coordinates are normalized by the nose radius ($R_N = 0.00508$ *m*).

A common misconception is that methods for assessing the discretization error based on Richardson Extrapolation are valid for uniform grids only. Extrapolation-based methods can be used to analyze problems on curvilinear, stretched, and skewed meshes using finite-differences provided the metric transformation to computational space is of the same order (or higher) as the numer-

ical scheme. This result also holds for finite-volume and finite-element schemes since the former can be shown to be mathematically equivalent to a coordinate transformation and the latter employs local coordinate transformations. However, problems can occur when a poor choice of transformations is made, and when the mesh is highly irregular. For the problems examined herein, where the meshes are curvilinear with little skewness or mesh stretching, the errors introduced by the effective transformation are expected to be negligible.

Iterative Convergence Errors

Iterative convergence was assessed by monitoring the L_2 norms of the residuals for the governing equations. The residual is defined by substituting the current solution into the steady state form of the discretized governing equations (i.e., without the time derivatives). The residuals will approach zero as a steady state solution is reached and the current solution satisfies the discretized form of the steady equations. For all equations on each mesh level the residuals were reduced down to machine zero (approximately fourteen orders of magnitude). For a similar case which included viscous effects, Roy et al.[18] showed that a reduction in the L_2 norms residuals corresponds directly to a drop in the error for the surface quantities. The reduction of the steady-state residuals to machine zero provides confidence that the iterative convergence errors will be small and therefore have a negligible impact on assessing grid convergence errors.

Grid Convergence Error Analysis

The order of accuracy for the surface pressure distributions has been calculated using Eq. (18) with Meshes 1, 2, and 3, and $r = 2$. Recall that the underlying assumption for this equation is that the solutions are in the asymptotic convergence range and therefore change monotonically as the grid is refined. The results, shown in Fig. 4, indicate that the local order of accuracy varies from

large negative values to values as large as eight. The undefined values, which are not included in the figure, occur when the argument of the natural logarithm in Eq. (18) is negative (i.e., the solutions are not monotonic). The failure of Eq. (18) to provide an "observed" order of accuracy close to the formal order of the scheme (second order) provides the motivation for the current work.

The next step towards understanding the order of accuracy of the method is to examine the behavior of some norms of the spatial error. In order to calculate error norms, local estimates of the exact solution are required. Estimates of the exact solution were obtained by extrapolating the solutions using Meshes 1 and 2 using the first-order extrapolation method obtained from Eq. (11) with $r = 2$ and $p = 1$. The L_1 and L_2 norms were then calculated from Eqs. (26). In addition, all of the norms employed only one-fourth of the available flowfield points from the body out towards the shock. The omission of the shock wave was required since the extrapolation technique used to approximate f_{exact} is not valid through discontinuities.

These norms are presented in Fig. 5 for the pressure and are plotted versus the grid cell size h on a log-log plot. Recall that the cell size was normalized such that $h = 1$ on the finest mesh (Mesh 1). Since a grid refinement factor of two (grid halving) was used, the discrete solutions fall at 1, 2, 4, 8, 16, 32, 64, and 128. The pressure norms exhibit a region of second-order behavior on the coarse meshes which quickly asymptotes to a first-order slope on the finer meshes. The first-order asymptotic behavior as the mesh is refined is expected, as discussed in the introduction.

The surface pressure will now be examined locally on a point-by-point basis. The behavior of the surface pressure with mesh refinement is presented in Fig. 6 at the sphere-cone tangency point ($x/R_N = 0.83$). It is seen that the pressure converges monotonically as the grid is refined (i.e., as $h \rightarrow 0$). The solid line at a value of $p = 1870\ N/m^2$ represents an estimate of the exact solution found from Eq. (23) using Meshes 1, 2, and 3 only.

Further insight into the error behavior can be gained by examining the contributions of both the first- and second-order error terms. Figure 7 shows the behavior of the grid convergence error in the surface pressure at the sphere-cone tangency point as the mesh is refined. The discrete solution error is calculated using the third-order accurate estimate $\tilde{f}_{exact}$ from Eq. (23) (using Meshes 1, 2, and 3) and the following relationship:

$$|\text{Spatial Error (\%)}| = \left| \frac{f_k - \tilde{f}_{exact}}{\tilde{f}_{exact}} \right| \times 100 \tag{27}$$

The discrete error is represented by the square symbols in Fig. 7 and is expected to be a good representation of the true error, especially for the coarser meshes. The reason is that the errors on the finest meshes are so small that similar coarse grid errors will result regardless of whether f_{exact} is approximated by first-, second-, or mixed-order extrapolation on the fine grids.

Also shown individually in the figure are the normalized magnitudes of the first- and second-order error terms

$$\left| \frac{\tilde{g}_1 h}{\tilde{f}_{exact}} \right| \times 100 \quad \text{and} \quad \left| \frac{\tilde{g}_2 h^2}{\tilde{f}_{exact}} \right| \times 100 \tag{28}$$

along with the magnitude of their sum:

$$\left| \frac{\tilde{g}_1 h + \tilde{g}_2 h^2}{\tilde{f}_{exact}} \right| \times 100 \tag{29}$$

The first-order error term has a slope of unity on the log-log plot. For a first-order scheme, this first-order error term will dominate the second-order error term as the mesh is refined. The second-order error term has a slope of two, and will dominate the total error when the scheme is exhibiting second-order behavior. The magnitude of the sum of the two terms (solid line) is forced

to pass through the points associated with Meshes 1, 2, and 3 since these solutions are used in the determination of the coefficients in Eqs. (21)-(23). First-order accuracy is seen in the fine grid solutions, while the error analysis predicts that the coarse grid solutions will begin to exhibit a second-order behavior. The grid convergence analysis, which uses only Meshes 1, 2, and 3, provides a reasonable prediction of the error on all meshes.

The behavior of the surface pressure as the mesh is refined is presented in Fig. 8 for the $x/R_N = 0.23$ location which is near the stagnation point. In this case, the pressure values first decrease as the grid is refined and then increase below $h = 16$; thus, a local minima occurs in the surface pressure occurs near $h = 16$ as the grid is refined. In this case, the surface pressure asymptotes to approximately 12980 N/m^2 on the finer meshes.

The spatial error as the grid is refined is presented in Fig. 9 for $x/R_N = 0.23$. The discrete values exhibit a first-order behavior on the finer meshes, but a second-order behavior on the coarser meshes. The coefficients of the first- and second-order error terms ($\tilde{g}_1$ and $\tilde{g}_2$) in this case are of opposite sign, thus giving error cancellation when $\tilde{g}_1 h = -\tilde{g}_2 h^2$. This error cancellation manifests as a sharp drop in the error "predicted" from using Meshes 1, 2, and 3 (solid line) at $h = 20$. It is the cancellation between the two leading error terms (first and second order in this case) which is responsible for the non-monotonic behavior of the pressure with mesh refinement. On the coarser grids, the second order term dominates and is positive (i.e., the solutions approach the asymptotic value from above). On the finer grids, the first order term dominates and is negative (i.e., the solutions approach the asymptotic value from below).

The mixed-order error analysis method has also been applied to the forebody drag, an integrated quantity. Figure 10 gives the behavior of the drag as the mesh is refined. A non-monotonic behavior is seen near $h = 32$. The drag values asymptote to approximately 0.99 N on the finer

meshes. The spatial errors in the drag are presented in Fig. 11. Good qualitative agreement is again observed between the error analysis (using only Meshes 1, 2, and 3) and the discrete solution error on all meshes. In fact, the location where the discrete solution error crosses over the estimated exact solution shown in Fig. 10 (between $h = 32$ and $h = 64$) is also captured by the error analysis, showing up in Fig. 11 as a sharp drop in the predicted error near $h = 42$. This examination of the drag shows that non-monotonic behavior can occur for global quantities as well. The non-monotone grid convergence behavior demonstrated for this relatively simple flow could certainly occur in more complex flows (e.g., flow separation, shock-boundary layer interaction, etc.), especially outside of the asymptotic grid convergence range.

Grid Convergence Error Estimators

In the previous section, the focus was on error analysis and, specifically, on understanding how and why non-monotonic behavior can occur for solution variables as the mesh is refined. In this section, the focus now shifts to error estimation. The error estimation methods discussed below are intended to be used for engineering calculations where only a limited number of grid levels are available. Both Roache[8] and Oberkampf and Blottner[38] encourage the use of at least three grid levels for problems sufficiently different than those previously studied. This position is also taken by the current author. If the three solutions converge monotonically as the mesh is refined, then the observed order of accuracy can be calculated with Eq. (18), and the generalized Richardson Extrapolation procedure of Eq. (17) can be employed using the two finest mesh levels. If the solutions do not converge monotonically, then the procedures developed in this section are recommended.

The goal of this section is to examine the behavior of a number of different error estimators for the hypersonic blunt-body flow currently under investigation. The ideal error estimator would

provide an error estimate that is very close to the actual error and carries some statistical measure of the confidence that the error estimate will be conservative (e.g., a 2σ or 95% confidence band). For complicated, nonlinear problems in multiple dimensions (and rarely in the true asymptotic grid convergence range), a rigorous proof of such an error band is probably not attainable.[5,8] One is therefore forced to rely on more heuristic methods of quantitatively assessing grid convergence errors.

The most straightforward error estimation method would be to simply use the extrapolated estimate of f_{exact} to estimate the error in the discrete solutions. For example, if the observed order of accuracy of some solution variable has been verified (and the solutions are monotonic), then the generalized Richardson Extrapolation can be used to estimate the error from Eq. (27). However, one does not necessarily know whether the estimated f_{exact} will be larger or smaller than the true exact solution. That is, $\tilde{f}_{exact}$ could approach f_{exact} either from above or from below (or even possibly in a non-monotonic manner depending on whether the solutions are asymptotic). One approach to insure conservative error estimates would be to add a factor of safety to the error estimate of Eq. (27), such as

$$|\text{Spatial Error (\%)}| = F_s \left| \frac{f_k - \tilde{f}_{exact}}{\tilde{f}_{exact}} \right| \times 100 \tag{30}$$

where this factor of safety can be chosen as some appropriate value (e.g., $F_s = 3$).

Another common approach to reporting grid convergence studies is to report the difference between a coarse grid solution f_2 and a fine grid solution f_1. These differences are generally reported as some percentage of the fine grid value. Roache[8] points out the main problem with this approach is that the error estimate is independent of the order of accuracy of the numerical method and the grid refinement factor used. Clearly the true errors would be quite different if a 5% dif-

ference is found using this method for a first-order scheme versus a third-order scheme. A similar statement can be made for two cases where the grid refinement factor was $r = 2$ versus $r = 1.1$. Roache has proposed a uniform method for reporting grid convergence studies which properly accounts for the order of accuracy of the method and the grid refinement factor.[8] Roache's Grid Convergence Index (*GCI*), on a percentage basis, can be written as

$$GCI(\%) = \frac{F_s}{r^p - 1}\left|\frac{f_2 - f_1}{f_1}\right| \times 100 \tag{31}$$

where p is the order of the scheme, r is the grid refinement factor, and the factor of safety is generally taken to be $F_s = 3$. It can be shown that Eqs. (30) and (31) produce similar error estimates when the generalized Richardson Extrapolation method is used to determine $\tilde{f}_{exact}$ in Eq. (30) and when the *GCI* error estimate is less than 10-20% (see the Appendix B of Ref. 19 for details). It should be noted that all of these error estimators must be normalized by some reference value (other than $\tilde{f}_{exact}$) when $\tilde{f}_{exact}$ (or f_1 for the *GCI*) approaches zero.

Five different methods will be used to estimate the grid convergence errors. The first three methods all employ Eq. (30) without the factor of safety, but differ in that the estimate of the exact solution $\tilde{f}_{exact}$ is taken to be either **1)** the mixed $1^{st} + 2^{nd}$-order estimate of Eq. (23), **2)** the generalized Richardson Extrapolation value of Eq. (11) with $p = 1$, or **3)** the generalized Richardson Extrapolation value of Eq. (11) with $p = 2$. The remaining two methods which will be presented are Roache's *GCI*(%) assuming either **4)** first order ($p = 1$) or **5)** second order ($p = 2$), again without the factor of safety (i.e., the *GCI* is divided by three). The mixed-order method required three solutions to obtain the estimate of the exact solution, and the coarser meshes are used to provide these two additional solutions. For example, the mixed-order estimate at Mesh 4 ($h = 8$) will use the discrete solutions on Meshes 4, 5, and 6. The other estimators all require a single addition-

al coarse grid, thus estimates are available on all but the coarsest mesh. For example, the error estimates at Mesh 3 ($h = 4$) use discrete solutions on Meshes 3 and 4. These estimates are compared to the best estimate error, which is determined using the mixed-order extrapolation method on the three finest mesh solutions (Meshes 1, 2, and 3). This best estimate error is expected to be a very good error estimate, especially on the coarser meshes.

Evaluation of Error Estimators

The five error estimators discussed above are applied to the discrete values for the surface pressure at the $x/R_N = 0.83$ axial location for the various mesh levels, with the results shown in Fig. 12. For this case, the first-order error estimation methods provide conservative estimates of the error over the entire range of grids, while the mixed-order and second-order estimates are not always conservative. The differences between the first-order extrapolation of Eq. (30) and the first-order *GCI*(%) are evident only when the *GCI*÷3 is larger than approximately 4% (i.e., the *GCI* is larger than 12%). This behavior is discussed in detail in the Appendix. It should be noted that the first-order *GCI* and the second-order *GCI* will, by definition, differ only by a factor of three (see Eq. (31)).

The error estimation results at $x/R_N = 0.23$ are given in Fig. 13. In this case, the mixed-order error estimator most closely matches the actual error behavior. This result is expected since the pressure showed a clear non-monotonic behavior at this location, with a local minimum occurring at $h = 16$. In regions of non-monotonic grid convergence, the single-order error estimators are prone to extrapolate with the wrong slope, or even in the wrong direction, and thus provide very poor estimates of the error.

Based on the above results, none of the error estimators have been shown to provide superior error estimates in all cases. In general, the first-order error estimator (along with the first-order

GCI) provided the best results when the properties converged monotonically with grid refinement; conversely, the mixed-order error estimator was clearly superior when the properties converged non-monotonically with grid refinement. Both of these error estimators performed well when the error was small (i.e., on the finer meshes).

Application of the Mixed-Order Error Estimator

The mixed-order extrapolation method will now be applied to surface and field pressure of the current simulations using Meshes 1, 2, and 3. The error estimates on the fine grid for the surface pressure are presented in Fig. 14. The error is fairly constant at -0.08% for $x/R_N < 0.25$ and $x/R_N > 1.5$. In between, the error oscillates between approximately -0.25% and 0.1%. The source of the oscillatory error will be discussed in the following paragraph. The maximum errors occur near the sphere-cone tangency point (+0.5% and -1.4%). The relatively large errors at the sphere-cone tangency point are due to the fact this point is a surface curvature discontinuity. In general, such singular points should be addressed either by additional grid refinement or other special treatment.

The field errors in the pressure for Mesh 1 are shown in Fig. 15, again using the mixed-order method to approximate the exact solution. While the errors were by far the largest at the shock wave due to the poor estimate of the exact solution in the presence of the shock discontinuity (note that the series expansion of Eq. (2) is not valid through a discontinuity), the contour levels were scaled to best illustrate the propagation of the error behind the shock wave. The errors at the shock wave exhibit an oscillatory behavior due the misalignment of the bow shock and the grid lines (recall that no effort was made to align or cluster the mesh to the shock). The errors at the shock wave propagate through the flow along local characteristics, reflect off the body, and then continue to travel along the characteristics to again reach the shock. As the errors from the shock

cross over the reflected errors, an interference pattern is created. It is the impingement of these propagated errors onto the surface that leads to the oscillatory behavior seen in the error in surface pressure (Fig. 14).

The relatively large errors observed in Fig. 14 at the sphere-cone tangency point ($x/R_N = 0.83$) are clearly shown in the field plot of Fig. 15. The error at the sphere-cone tangency point also propagates through the flowfield along a characteristic Mach line. The overall discretization error comes from two sources: local error and transmitted error (also known as pollution error). It is clear from Fig. 15 that extrapolation-based error estimators measure the discretization error (or global error), capturing the error propagated downstream from the shock. A good extrapolation-based error estimator can thus be used both for quantifying the discretization error in a given solution and for mesh adaption.

Summary and Conclusions

Results were presented for the Mach 8 inviscid flow of a calorically perfect gas over a spherically-blunted cone. A formally second-order numerical method was employed; however, the spatial order of accuracy of the method was reduced to first order at the shock wave via a flux limiting procedure in order to prevent numerical oscillations. The numerical scheme is therefore mixed-order in the sense that the order of the local truncation error (which determines the order of accuracy of the scheme) varies from second order over most of the domain to first order at the shock wave. The first-order truncation error at the shock wave led to the presence of a first-order discretization error component (however small) everywhere downstream. As the mesh spacing was refined, this first-order error component eventually dominated the total discretization error.

An error analysis method was presented for mixed-order numerical schemes in which both first- and second-order error terms were included. When the coefficients of these error compo-

nents had the same sign, the convergence of the solution properties as the mesh was refined was monotone. However, when these coefficients were of opposite sign, error cancellation occurred at the crossover point where $\tilde{g}_1 h = -\tilde{g}_2 h^2$, resulting in non-monotonic behavior in the solution variables. The proposed mixed-order error analysis captures the non-monotonic behavior of the solution variables.

An error estimator was proposed which used a mixed-order extrapolation to obtain an estimate of the exact solution. When the local solution was non-monotonic with grid refinement, this mixed-order error estimator was shown to provide good local estimates of the error. Methods based on single-order extrapolation provided poor error estimates in the presence of non-monotonic grid convergence. However, when the solution was monotone, the first-order error estimators provided the best error estimates. The error in the surface pressure was quantified using the mixed-order error estimator. The largest errors were found to occur near the sphere-cone tangency point and were approximately 1.4% in magnitude for the fine mesh (1024×512 cells). A field plot of the estimated error in the pressure showed an oscillatory behavior in the error at the shock wave due to grid misalignment, along with a relatively large error at the sphere-cone tangency point. The errors from both of these sources propagated downstream along characteristic Mach lines. The large errors at the sphere-cone tangency point were due to discontinuities in the local surface curvature and therefore require additional grid clustering.

Acknowledgments

A number of people made valuable contributions to this work. I would like to thank Fred Blottner and Bill Oberkampf of Sandia National Laboratories for their numerous discussions on grid convergence and error analysis. Thanks also go to Matthew Hopkins of Sandia National Laboratories for his helpful discussions on numerical analysis and applied mathematics. Finally, I

wish to thank Patrick Roache (consultant) who provided an extremely insightful review of many of the ideas presented herein. This work was supported by Sandia National Laboratories and the Department of Energy's Accelerated Strategic Computing Initiative. Sandia is a multiprogram laboratory operated by Sandia Corporation, a Lockheed Martin Company, for the United States Department of Energy under Contract DE-AC04-94AL85000.

References

1. "Best Practice Guidelines," ERCOFTAC Special Interest Group on Quality and Trust in Industrial CFD, M. Casey and T. Wintergerste, Eds., Jan. 2000.

2. Hutton, A. G., and Casey, M. V., "Quality and Trust in Industrial CFD - A European Initiative," AIAA Paper 2001-0656, Jan. 2001.

3. Harvey, J. K., Holden, M. S., and Wadhams, T. P., "Code Validation Study of Laminar Shock/Boundary Layer and Shock/Shock Interactions in Hypersonic Flow Part B: Comparison with Navier-Stokes and DSMC Solutions," AIAA Paper 2001-1031, Jan. 2001.

4. Freitas, C. J., "Perspective: Selected Benchmarks from Commercial CFD Codes," *ASME Journal of Fluids Engineering*, Vol. 117, June 1995, pp. 208-218.

5. Roache, P. J., *Verification and Validation in Computational Science and Engineering*, Hermosa Publishers, New Mexico, 1998.

6. *Guide for the Verification and Validation of Computational Fluid Dynamics Simulations*, AIAA G-077-1998, p. 3.

7. Anderson, D. A., Tannehill, J. C., and Pletcher, R. H., *Computational Fluid Mechanics and Heat Transfer*, Hemisphere Publishing, USA, 1984, pp. 89-92.

8. Roache, P. J., "Perspective: A Method for Uniform Reporting of Grid Refinement Studies," *ASME Journal of Fluids Engineering*, Vol. 116, Sept. 1994, pp. 405-413.

9. Godunov, S. K., "A Difference Scheme for Numerical Computation of Discontinuous Solution of Hydrodynamic Equat9ions," *Math. Sbornik*, 47, 271-306 (in Russian), Translated US Joint Publ. Res. Service, JPRS 7226 (1969).

10. Carpenter, M. H., and Casper, J. H., "Accuracy of Shock Capturing in Two Spatial Dimensions," *AIAA Journal*, Vol. 37, No. 9, 1999, pp. 1072-1079.

11. Efraimsson, G., and Kreiss, G., "A Remark on Numerical Errors Downstream of Slightly Viscous Shocks," *SIAM Journal of Numerical Analysis*, Vol. 36, No. 3, 1999, pp. 853-863.

12. Engquist, B., and Sjogreen, B., "The Convergence Rate of Finite Difference Schemes in the Presence of Shocks," *SIAM Journal of Numerical Analysis*, Vol. 35, 1998, pp. 2464-2485.

13. Efraimsson, G., Nordstrom, J., and Kreiss, G., "Artificial Dissipation and Accuracy Downstream of Slightly Viscous Shocks," AIAA Paper 2001-2608, June 2001.

14. Leonard, B. P., "A Stable and Accurate Convective Modelling Procedure Based on Quadratic Upstream Interpolation," *Computational Methods in Applied Mechanical Engineering*, Vol. 19, 1979, pp. 59-98.

15. Celik, I., and Zhang, W-M., "Calculation of Numerical Uncertainty Using Richardson Extrapolation: Application to Some Simple Turbulent Flow Calculations," *ASME Journal of Fluids Engineering*, Vol. 117, Sept. 1995, pp. 439-445.

16. Celik, I., and Karatekin, O., "Numerical Experiments on Application of Richardson Extrapolation with Nonuniform Grids," *ASME Journal of Fluids Engineering*, Vol. 119, Sept. 1997, pp. 584-590.

17. Roy, C. J., McWherter-Payne, M. A., and Oberkampf, W. L., "Verification and Validation for Laminar Hypersonic Flowfields," AIAA Paper 2000-2550, June 2000.

18. Roy, C. J., McWherter-Payne, M. A., and Oberkampf, W. L., "Verification and Validation for Laminar Hypersonic Flowfields Part 1: Verification," manuscript submitted to the *AIAA Journal*, February 2002.

19. Roy, C. J., "Grid Convergence Error Analysis for Mixed-Order Numerical Schemes," AIAA Paper 2001-2606, June 2001.

20. Wong, C. C., Soetrisno, M., Blottner, F. G., Imlay, S. T., and Payne, J. L., "PINCA: A Scalable Parallel Program for Compressible Gas Dynamics with Nonequilibrium Chemistry," SAND 94-2436, Sandia National Laboratories, Albuquerque, NM, 1995.

21. Wong, C. C., Blottner, F. G., Payne, J. L., and Soetrisno, M., "Implementation of a Parallel Algorithm for Thermo-Chemical Nonequilibrium Flow Solutions," AIAA Paper 95-0152, Jan. 1995.

22. Hassan, B., Kuntz, D. W., and Potter, D. L., "Coupled Fluid/Thermal Prediction of Ablating Hypersonic Vehicles," AIAA Paper 98-0168, Jan. 1998.

23. Kuntz, D. W., Hassan, B., and Potter, D. L., "An Iterative Approach for Coupling Fluid/Thermal Predictions of Ablating Hypersonic Vehicles," AIAA Paper 99-3460, June-July 1999.

24. Steger, J. L., and Warming, R. F., "Flux Vector Splitting of the Inviscid Gasdynamic Equations with Applications to Finite Difference Methods," *Journal of Computational Physics*, Vol. 40, 1981, pp. 263-293.

25. Van Leer, B., "Towards the Ultimate Conservative Difference Scheme. V. A Second Order Sequel to Godunov's Method," *Journal of Computational Physics*, Vol. 32, No. 1, 1979, pp. 101-136.

26. Yoon, S., and Jameson, A., "An LU-SSOR Scheme for the Euler and Navier-Stokes Equations," AIAA Paper 87-0600, Jan. 1988.

27. Yoon, S., and Kwak, D., "Artificial Dissipation Models for Hypersonic External Flow," AIAA Paper 88-3708, 1988.

28. Peery, K. M., and Imlay, S. T., "An Efficient Implicit Method for Solving Viscous Multi-Stream Nozzle/Afterbody Flow Fields," AIAA Paper 86-1380, June 1986.

29. Payne, J. L., and Hassan, B., "Massively Parallel Computational Fluid Dynamics Calculations for Aerodynamics and Aerothermodynamics Applications," Proceedings of the 1998 HPC-CP/CAS Workshop, NASA/CP-1999-208757, Jan. 1999, pp. 111-116.

30. Payne, J. L., and Walker, M. A., "Verification of Computational Aerodynamic Predictions for Complex Hypersonic Vehicles using the INCA^{TM} Code," AIAA Paper 95-0762, January 1995.

31. Roy, C. J., Gallis, M. A., Bartel, T. J., and Payne, J. L., "Navier-Stokes and DSMC Simulations for Hypersonic Laminar Shock-Shock Interaction Flows," AIAA Paper 2002-0737, Jan. 2002.

32. Roy, C. J., Gallis, M. A., Bartel, T. J., and Payne, J. L., "Navier-Stokes and DSMC Predictions for Laminar Hypersonic Shock-Induced Separation," manuscript to be submitted to the *AIAA Journal*, February 2002.

33. Richardson, L. F., "The Approximate Arithmetical Solution by Finite Differences of Physical Problems Involving Differential Equations with an Application to the Stresses in a Masonry Dam," *Transactions of the Royal Society of London*, Ser. A 210, 1908, pp. 307-357.

34. Richardson, L. F., "The Deferred Approach to the Limit," *Transaction of the Royal Society of London*, Ser. A 226, 1927, pp. 229-361.

35. de Vahl Davis, G., "Natural Convection of Air in a Square Cavity: A Bench Mark Numerical Solution," *International Journal for Numerical Methods in Fluids*, Vol. 3, No. 3, 1983, pp. 249-264.

36. Ralston, A., "Ch. 4. Numerical Differentiation, Numerical Quadrature, and Summation," *A First Course in Numerical Analysis*, McGraw-Hill, New York, 1965, pp. 118-124.

37. Roache, P. J., and Knupp, P. M., "Completed Richardson Extrapolation," *Communications in Numerical Methods in Engineering*, Vol. 9, 1993, pp. 365-374.

38. Oberkampf, W. L., and Blottner, F. G., "Issues in Computational Fluid Dynamics Code Verification and Validation," *AIAA Journal*, Vol. 36, No. 5, 1998, pp. 687-695.

Table 1 Flowfield conditions for the sphere-cone simulations

Flow Parameter	Value
Freestream Mach Number, M	8.0
Freestream Static Pressure, p	286.817 N/m^2
Freestream Static Temperature, T	47.668 K

Table 2 Flowfield meshes for the sphere-cone simulations

Mesh Name	Mesh Cells	Grid Spacing, h^a
Mesh 1	1024×512	1
Mesh 2	512×256	2
Mesh 3	256×128	4
Mesh 4	128×64	8
Mesh 5	64×32	16
Mesh 6	32×16	32
Mesh 7	16×8	64
Mesh 8	8×6	128

[a]The grid spacing measure is normalized by the grid spacing on the finest mesh (e.g., Mesh 1 has $h = 1$)

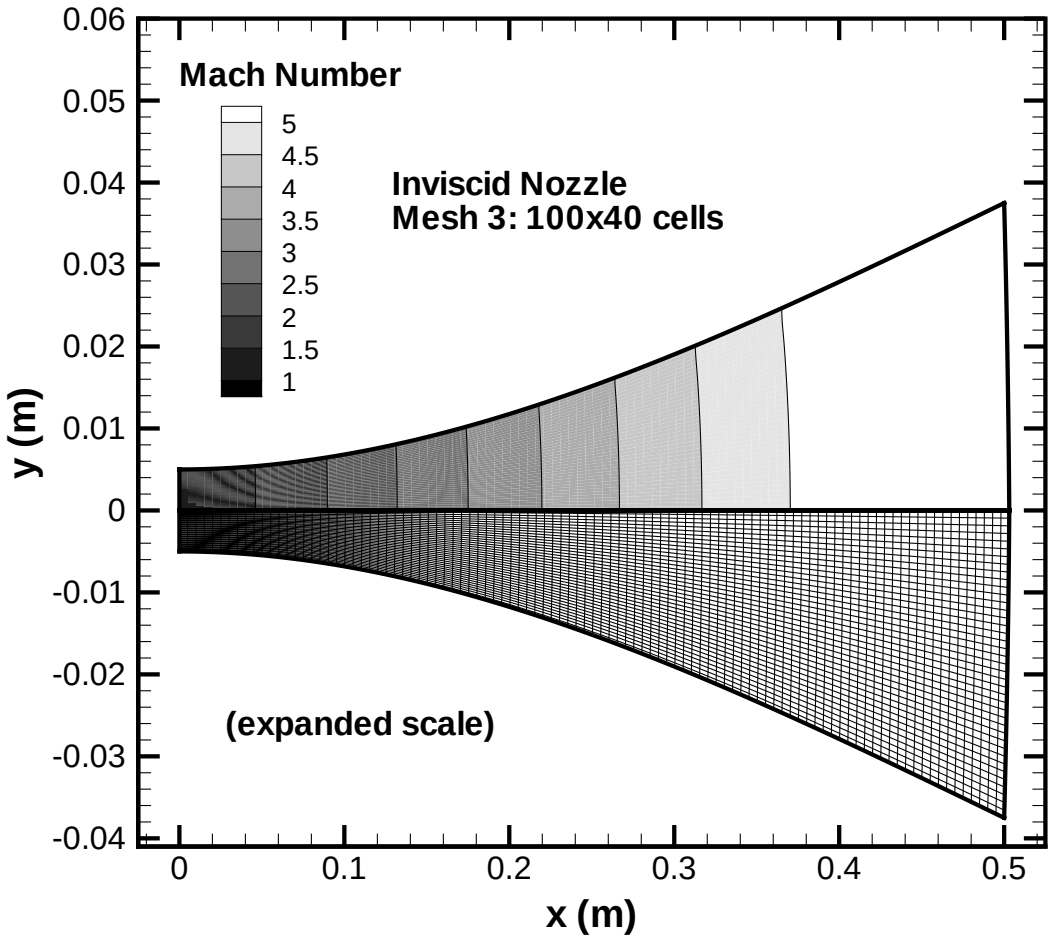

Fig. 1 Grid and Mach contours for the inviscid nozzle case.

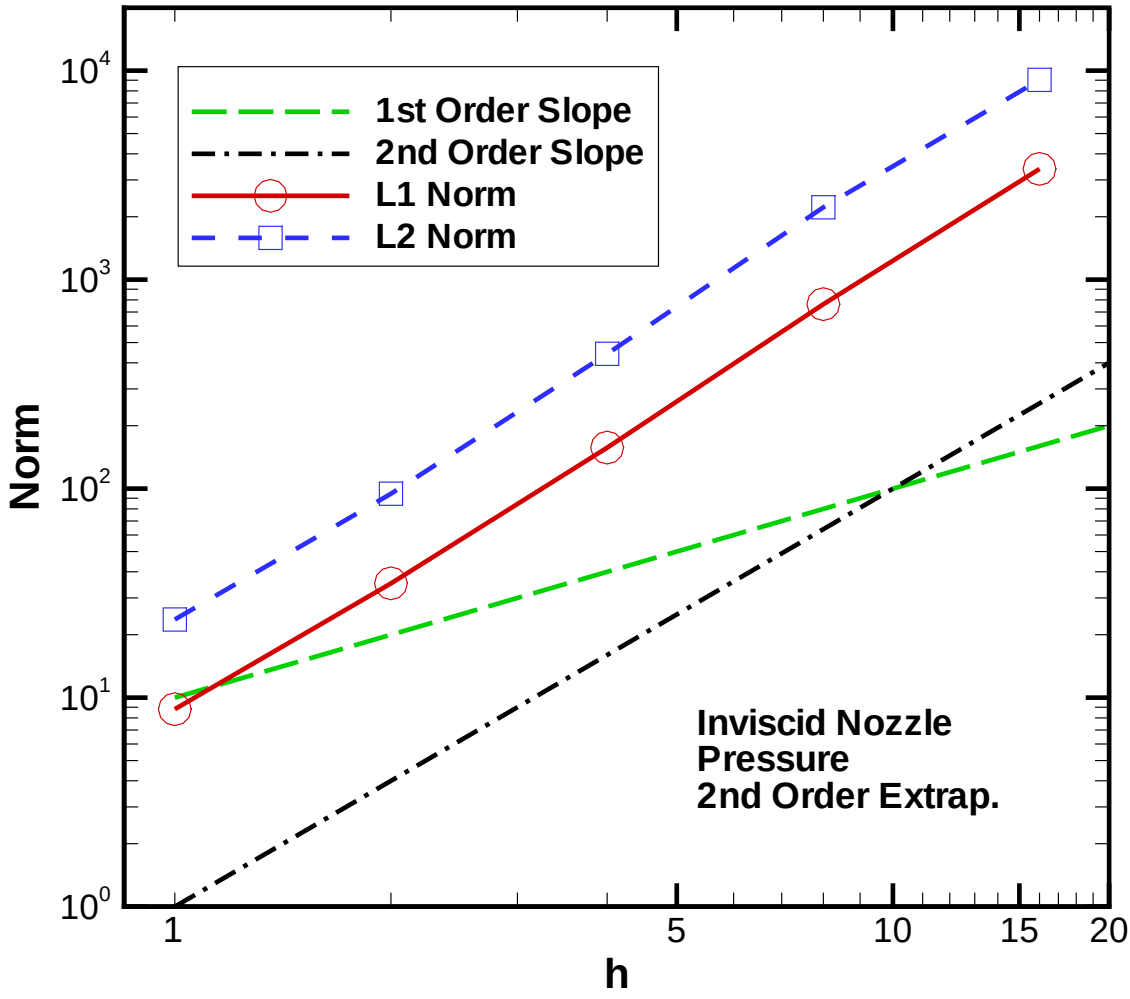

Fig. 2 Spatial error norms of pressure for the inviscid nozzle case.

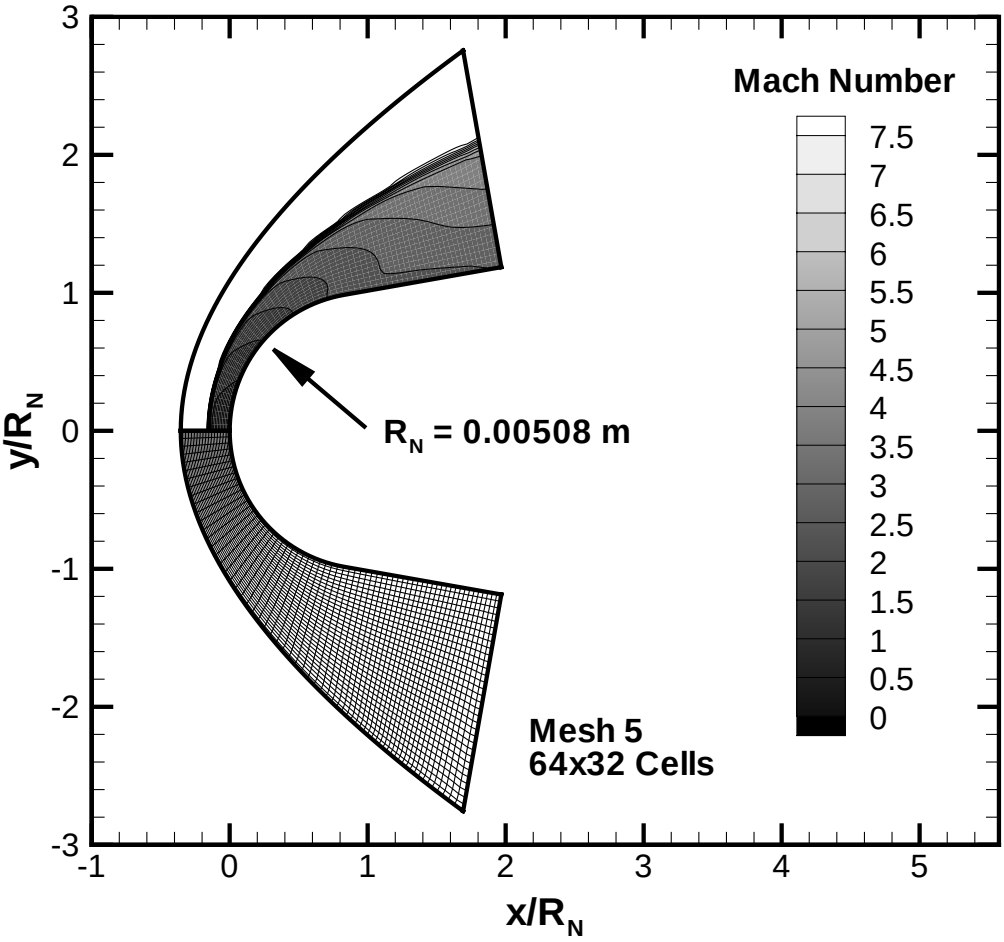

Fig. 3 Grid and Mach contours for inviscid sphere-cone.

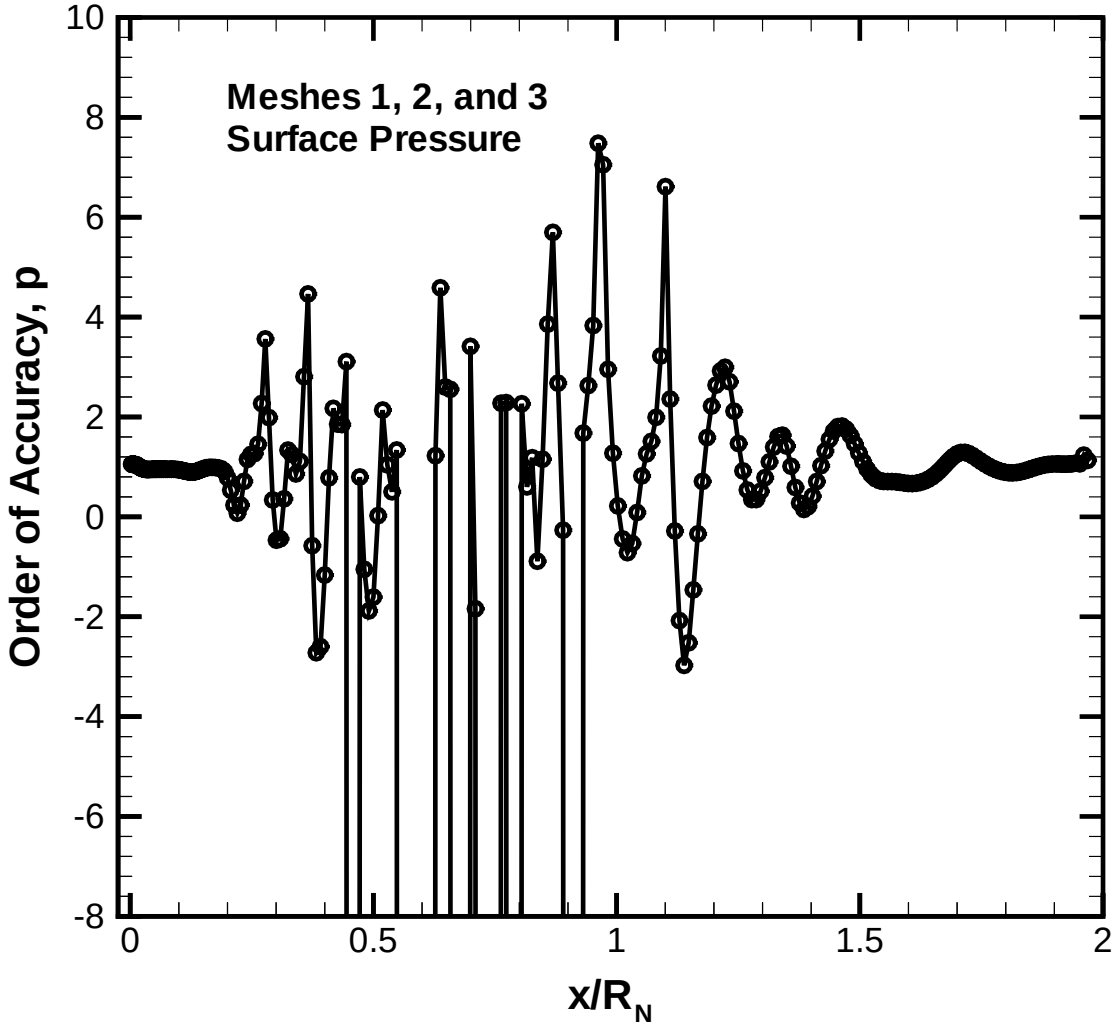

Fig. 4 Order of accuracy of the surface pressure distributions using Meshes 1, 2, and 3 and Eq. (18).

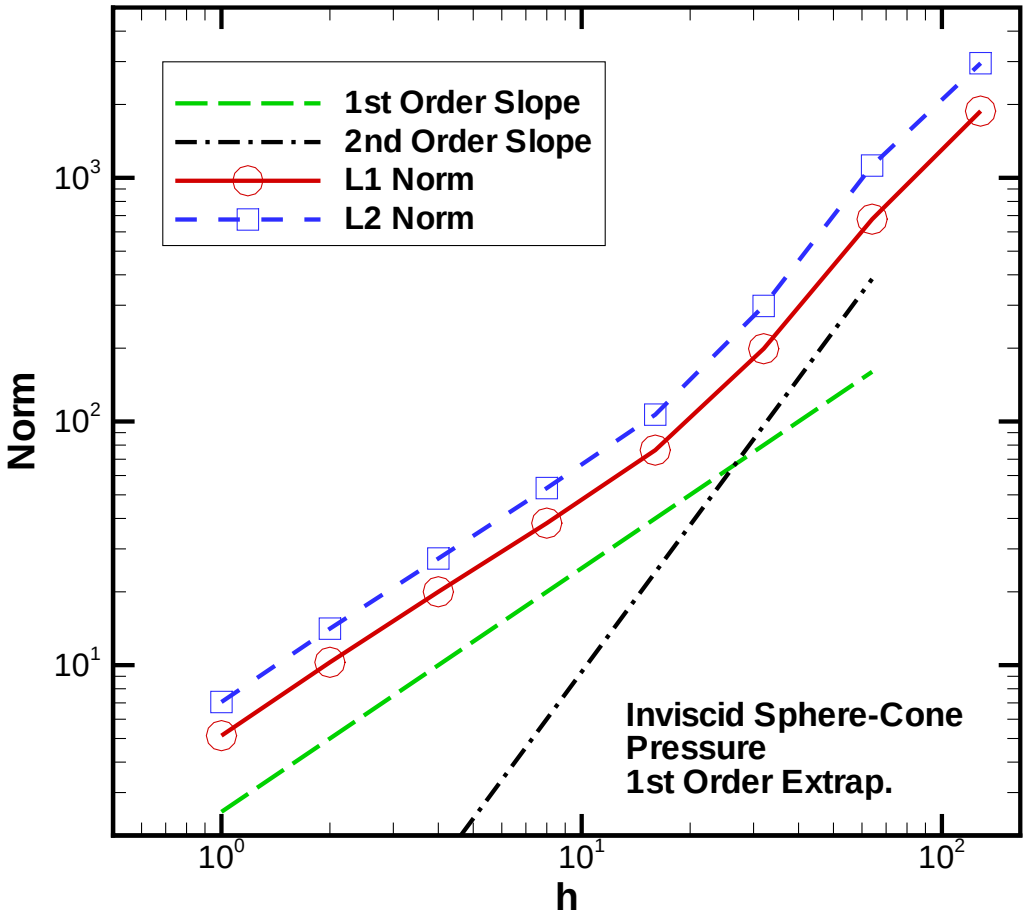

Fig. 5 Spatial error norms in pressure using one fourth of the points from the body to the outer boundary (excluding the shock).

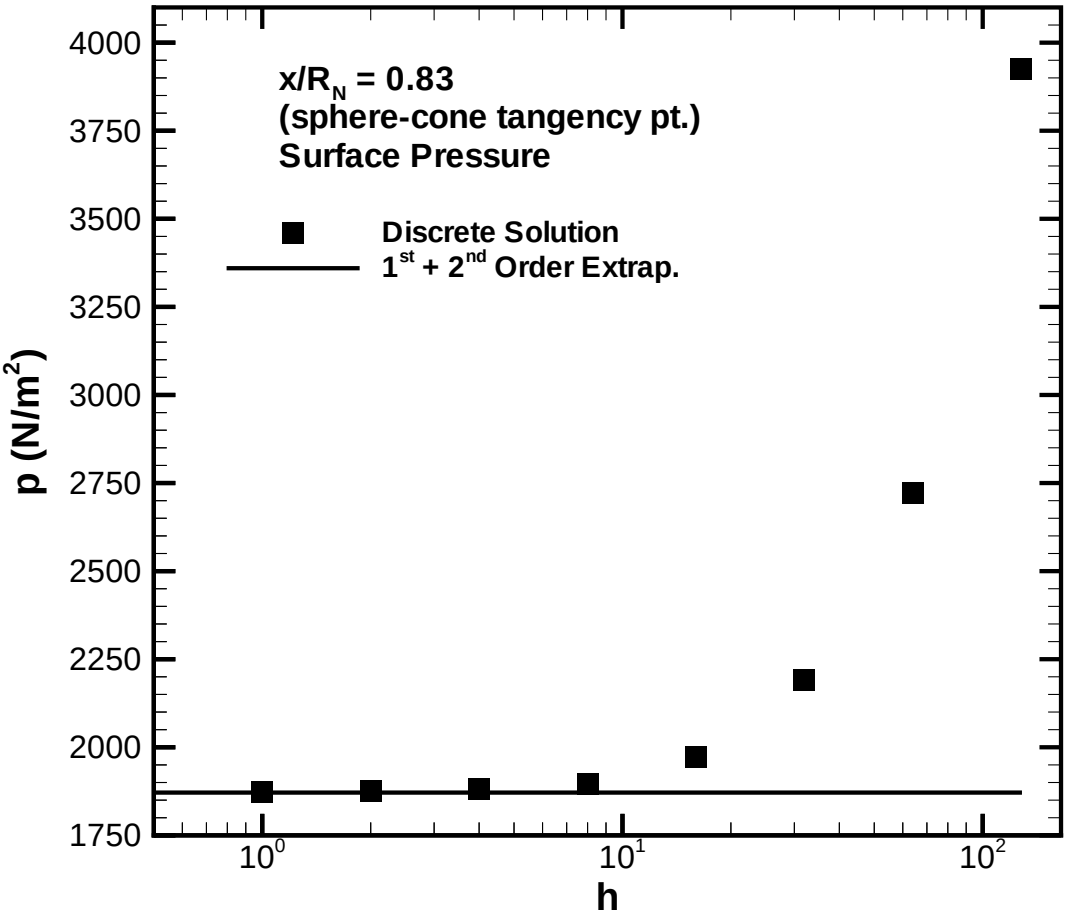

Fig. 6 Behavior of the surface pressure as the mesh is refined at the sphere-cone tangency point ($x/R_N = 0.83$).

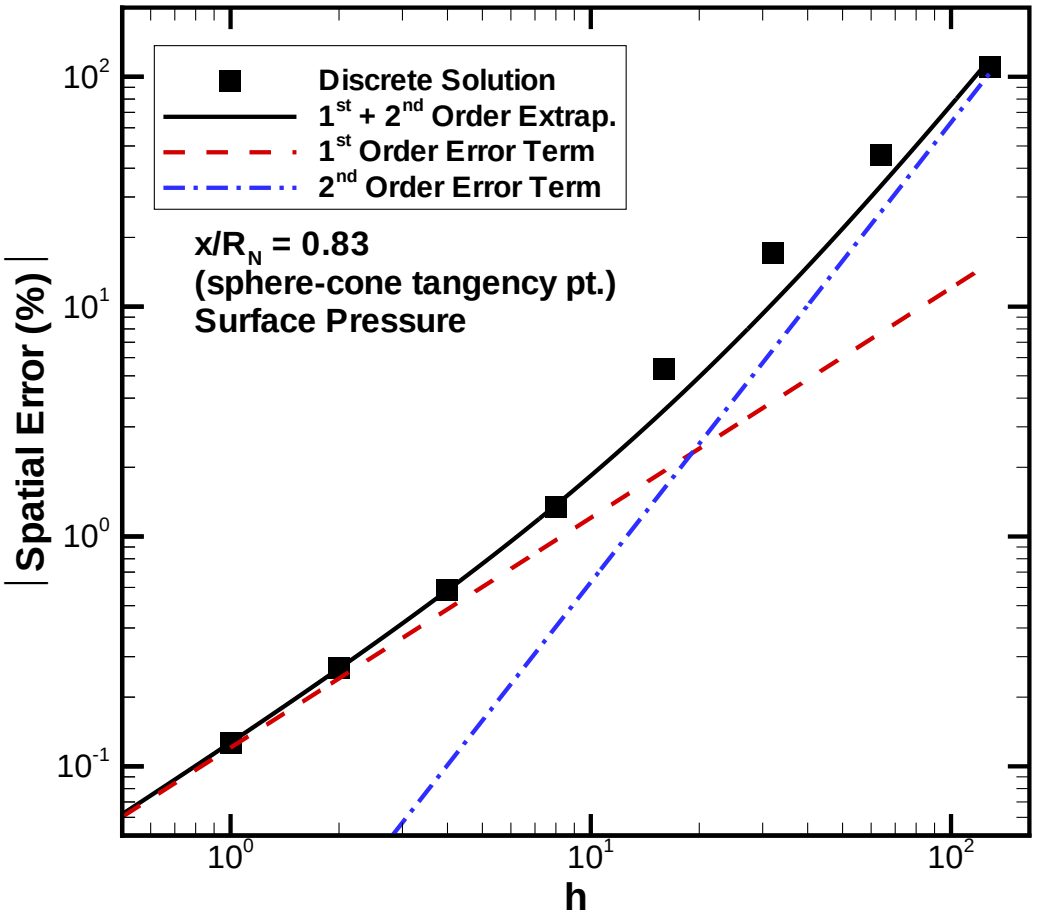

Fig. 7 Error in the surface pressure as the mesh is refined at the sphere-cone tangency point ($x/R_N = 0.83$).

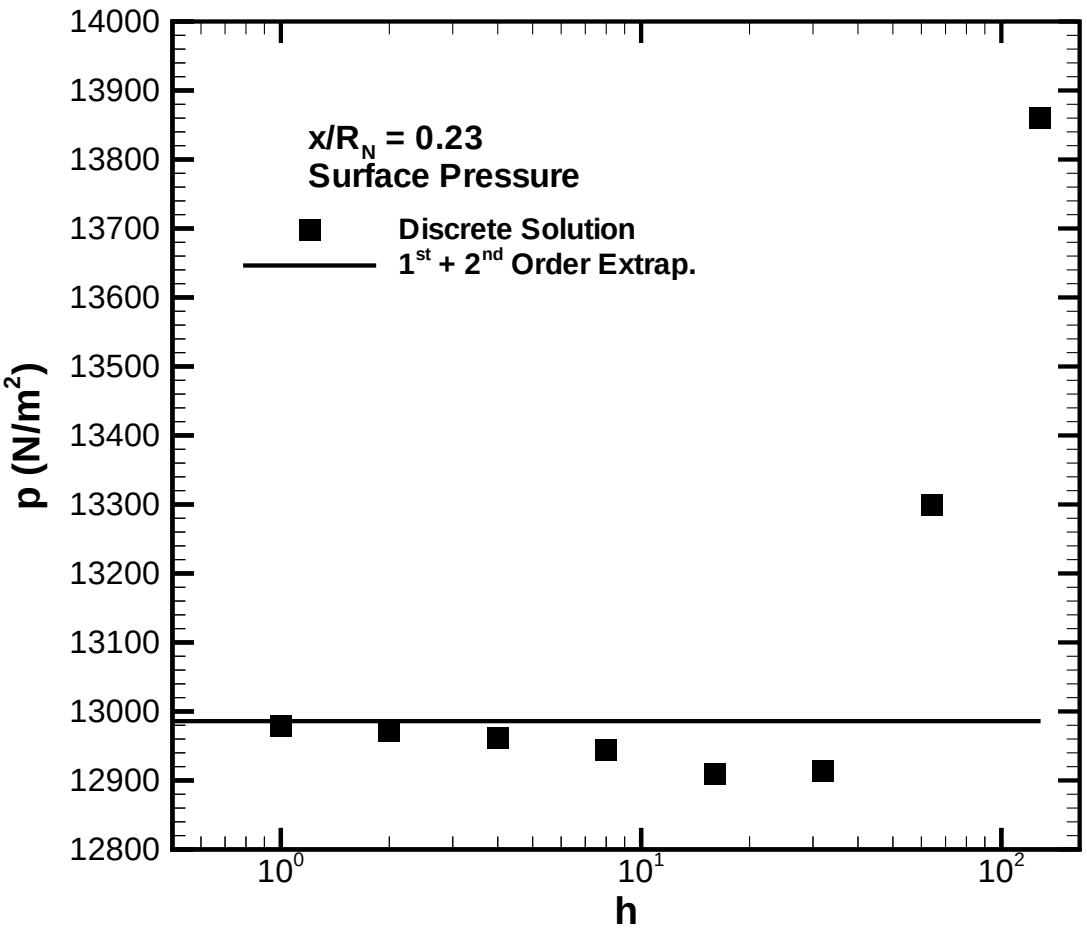

Fig. 8 Behavior of the surface pressure as the mesh is refined ($x/R_N = 0.23$).

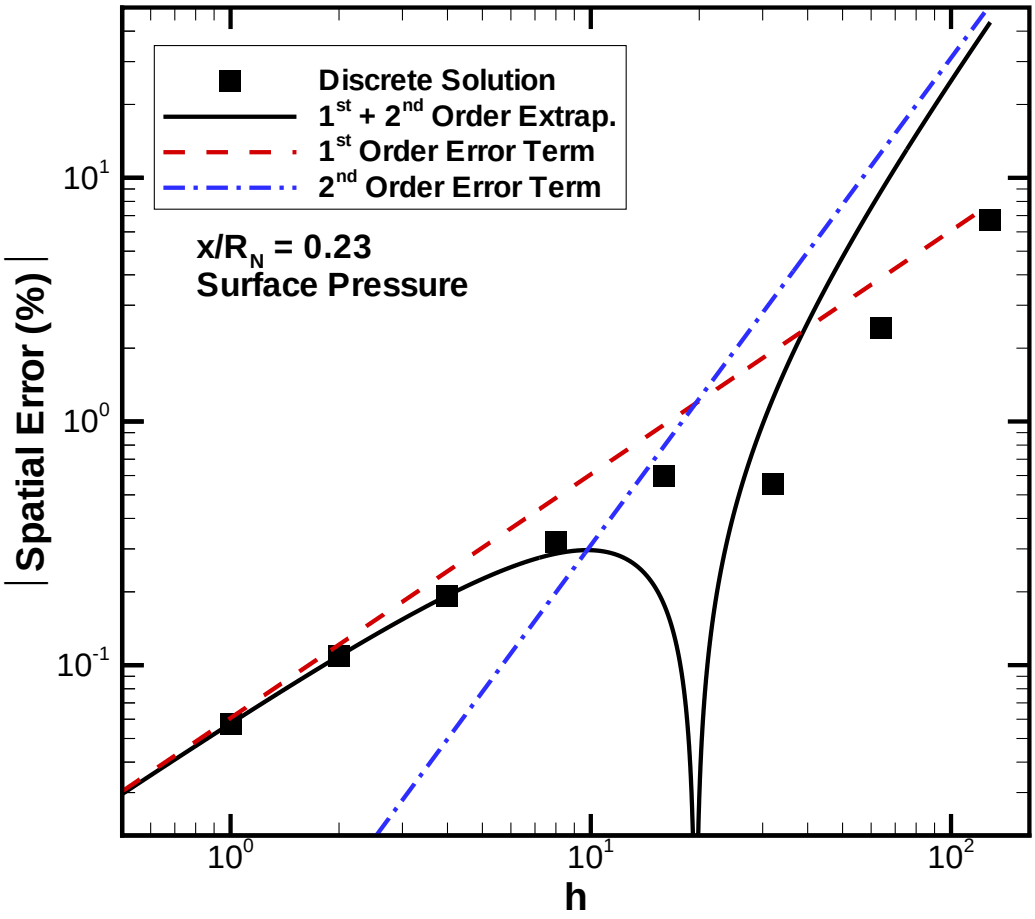

Fig. 9 Error in the surface pressure as the mesh is refined ($x/R_N = 0.23$).

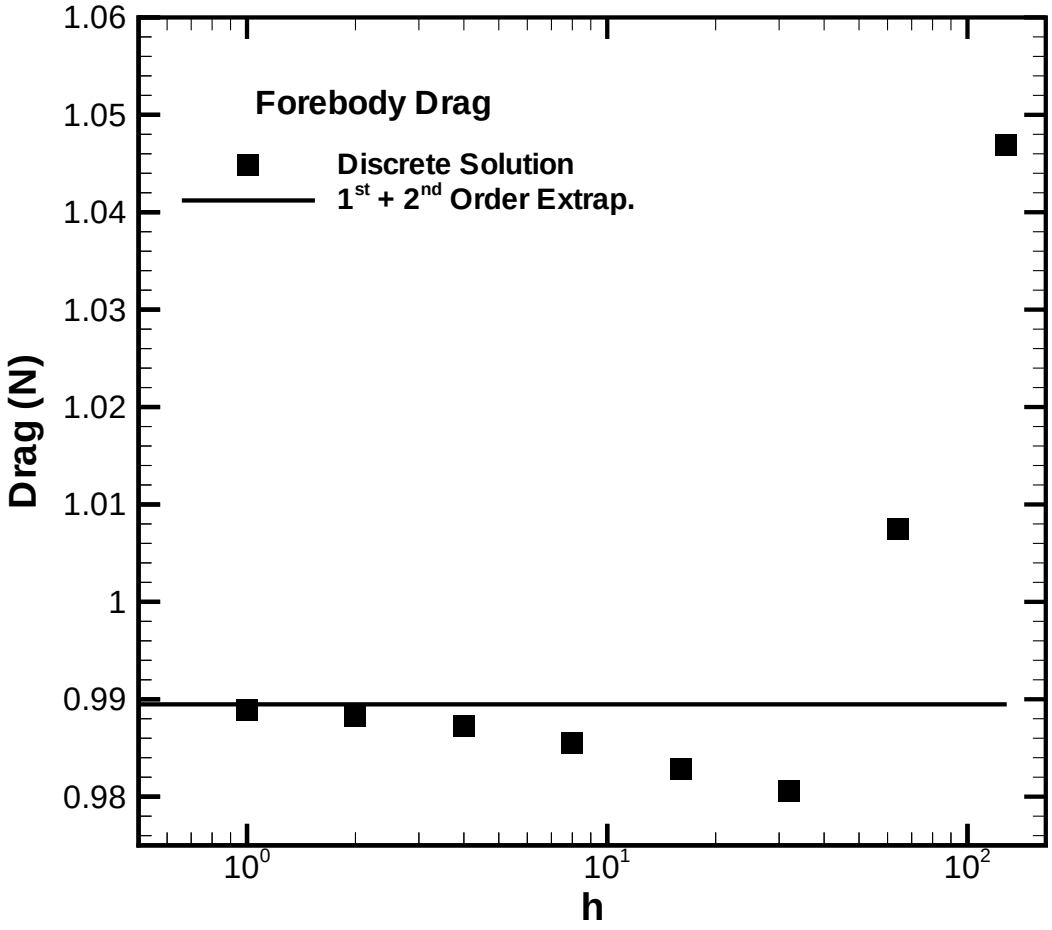

Fig. 10 Behavior of the forebody drag (excluding base drag) as the mesh is refined.

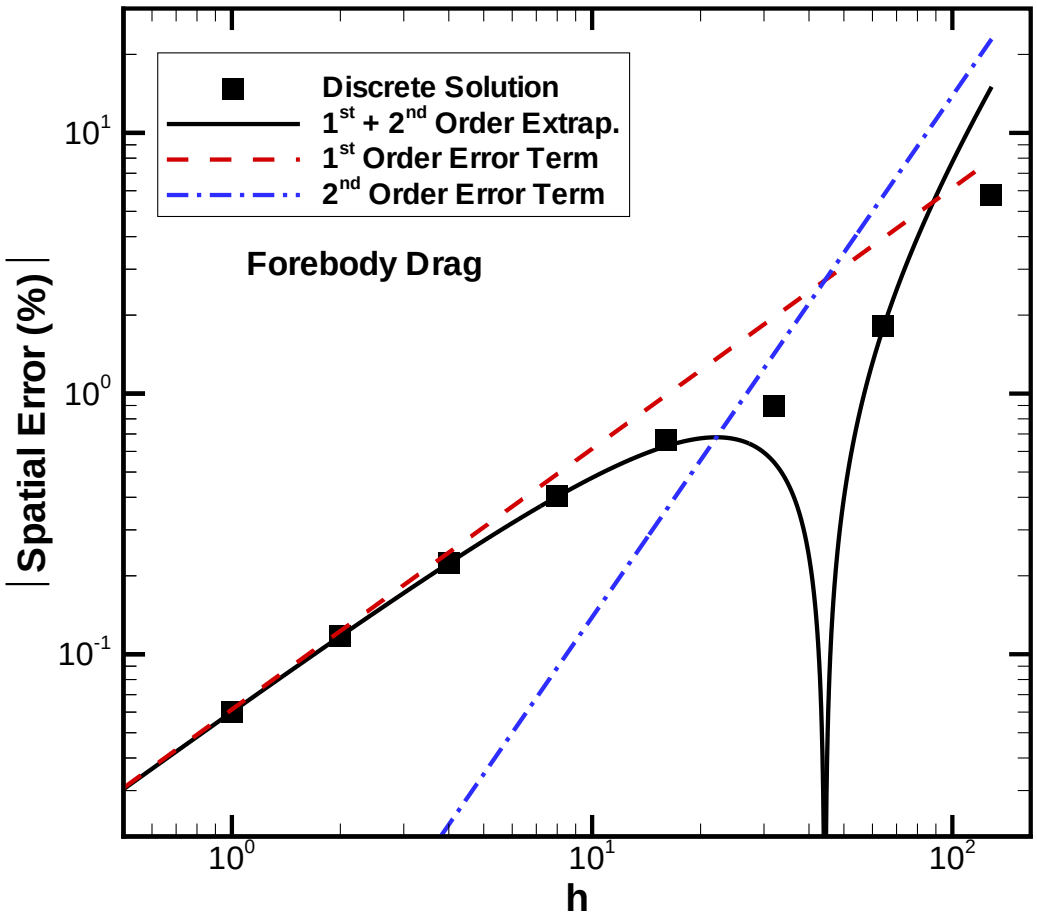

Fig. 11 Error in the forebody drag (excluding base drag) as the mesh is refined.

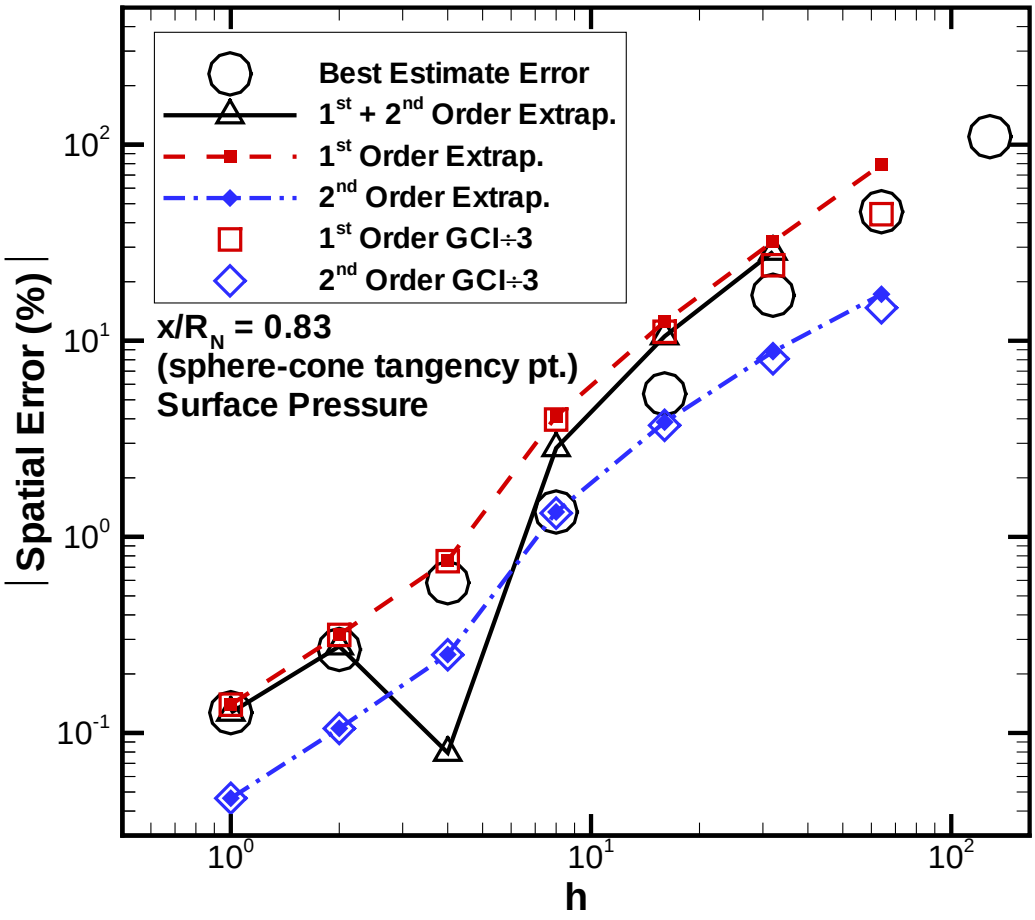

Fig. 12 Comparison of error estimates for the surface pressure at the sphere-cone tangency point ($x/R_N = 0.83$).

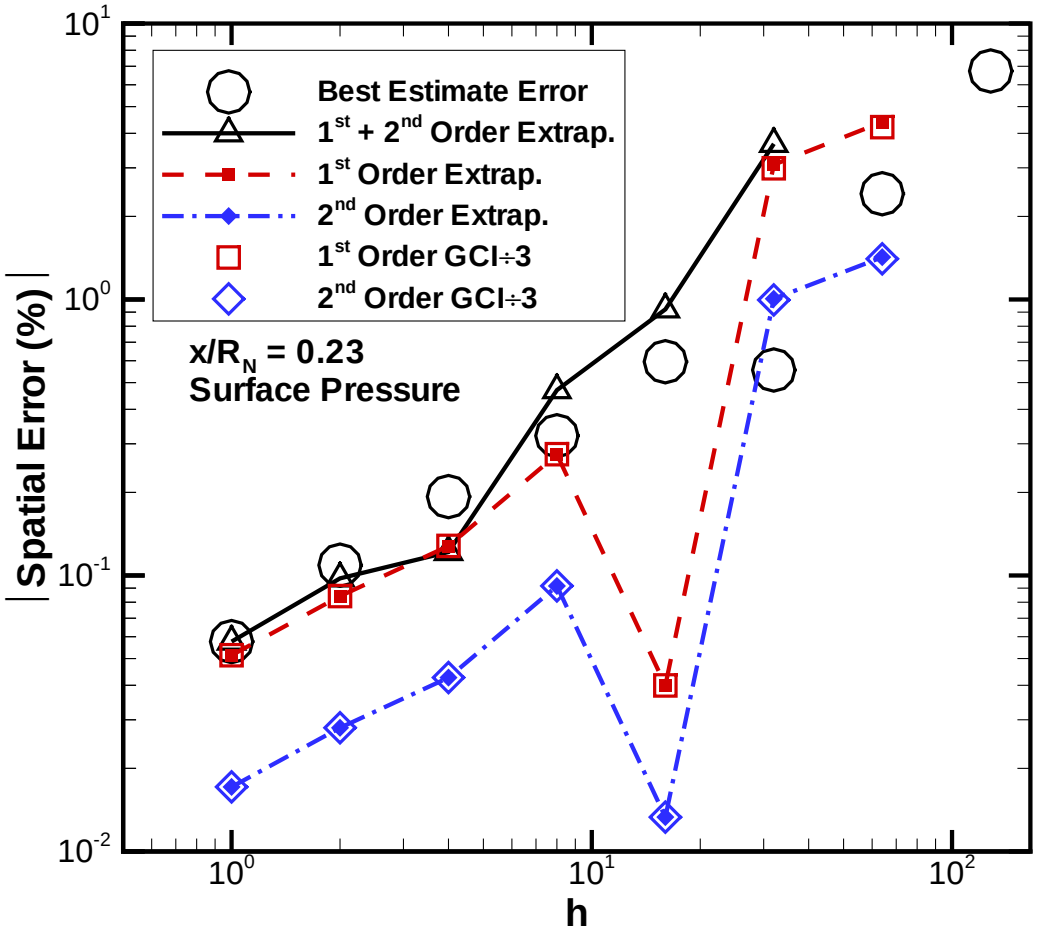

Fig. 13 Comparison of error estimates for the surface pressure ($x/R_N = 0.23$).

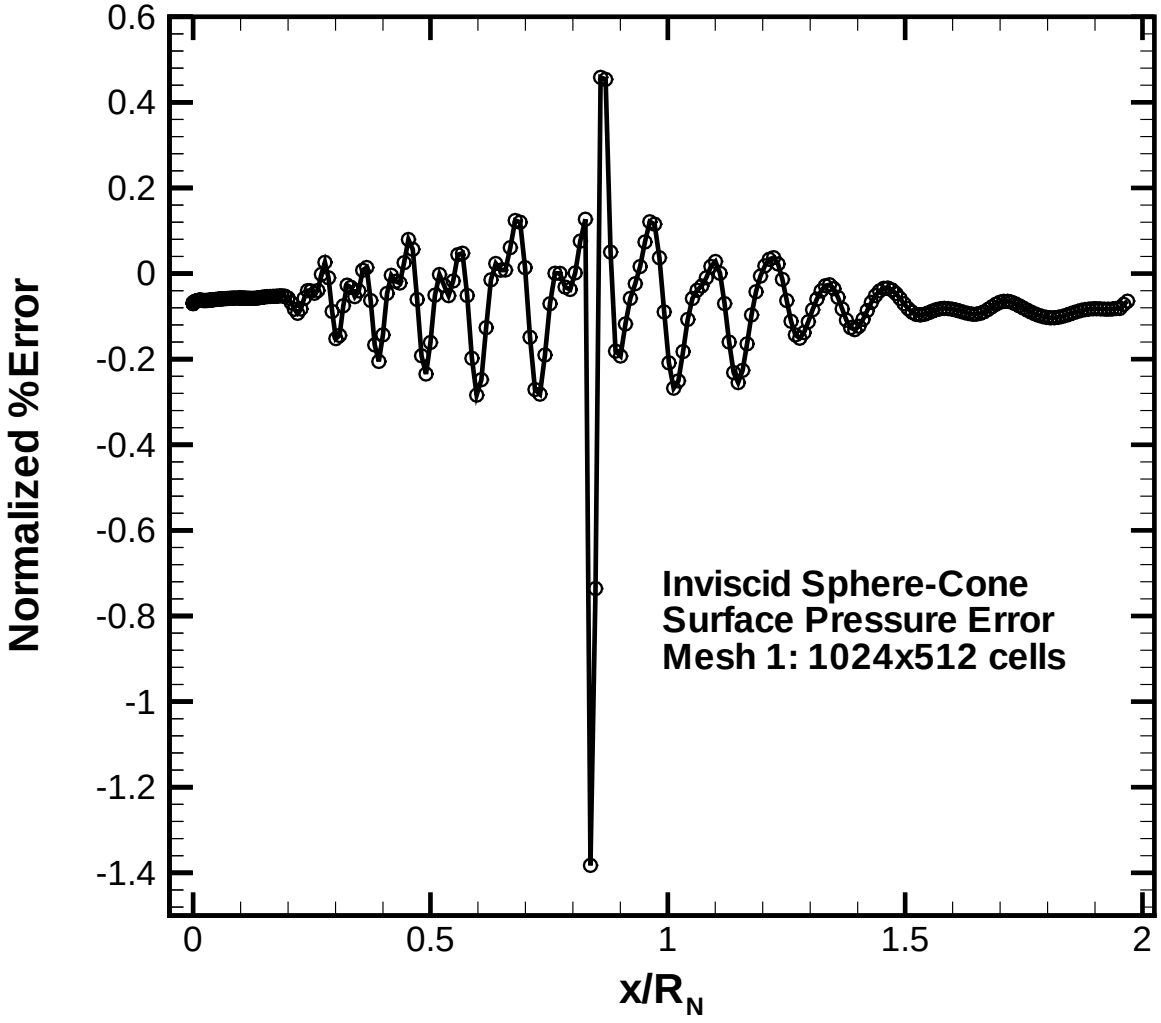

Fig. 14 Error estimates in the surface pressure for the inviscid sphere cone using Mesh 1 (1024×512 cells).

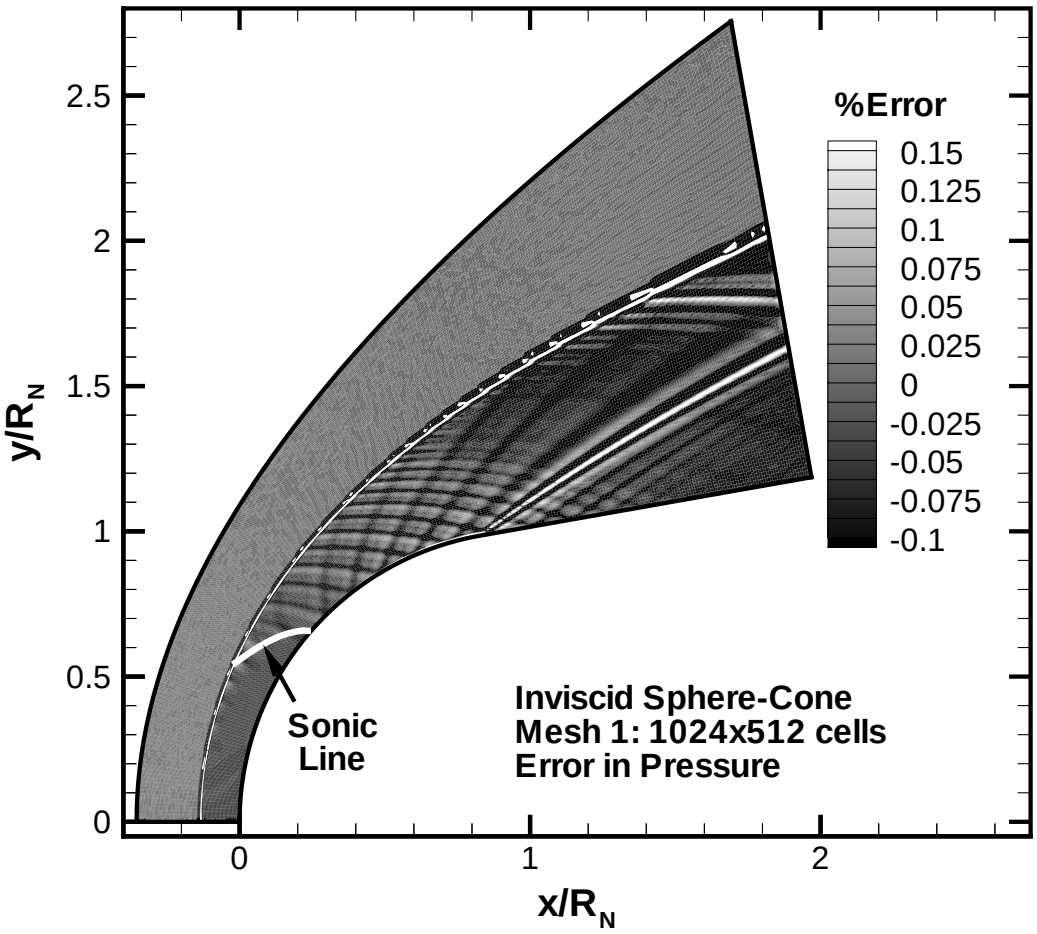

Fig. 15 Error estimates in pressure for the inviscid sphere-cone using Mesh 1 (1024×512 cells).